CHAPTER 11

CURRENT MEASUREMENTS USING A TILTING SPAR

by

R. L. Lowe, D. L. Inman and C. D. Winant

Scripps Institution of Oceanography, University of California

La Jolla, California 92037

ABSTRACT

The dynamic response of the spar to oscillatory flow has been examined by modeling as well as computer analysis of the non-linear differential equation. Field measurements using the tilting spar have been made. These measurements are compared with theory and with other more direct measurements of the wave field.

The tilting spar has been used to estimate wave direction. These estimates generally agree well with directional estimates made using a pressure sensor array and a two-component current meter.

INTRODUCTION

The tilting spar used in the Shelf and Shore (SAS) System (Lowe, Inman and Brush, 1972) is being used to measure horizontal currents. The SAS System is a general purpose data acquisition system for use in coastal waters. Instrumentation in the upper portion of the spar is used to measure low and high frequency oscillation. Thus, the shelf station (Figure 1) itself acts as a basic sensor.

The tilting spar section of the shelf station consists of a rigid, air filled, filament wound pipe, with a 8.9 cm outside diameter. The spar is coupled through a universal joint to the bottom anchor assembly so that it is free to tilt in any direction in response to horizontal currents. Motion is detected by accelerometers orthogonally mounted in the top section of the station. The signals from the accelerometers are digitized and telemetered to the shore station where they are analyzed.

MODEL STUDY

The shelf station is a forced, damped oscillator and as such will have a resonant frequency. A model study was conducted to determine if this resonant frequency could be observed.

A 1/7th scale model of the station was constructed and tested in the wind and wave channel at Scripps Institution of Oceanography. Displacements of the station were measured photographically and wave height and period were measured using digital wave staffs. The model was driven by waves of periods from 2.0 to 9.0 seconds.

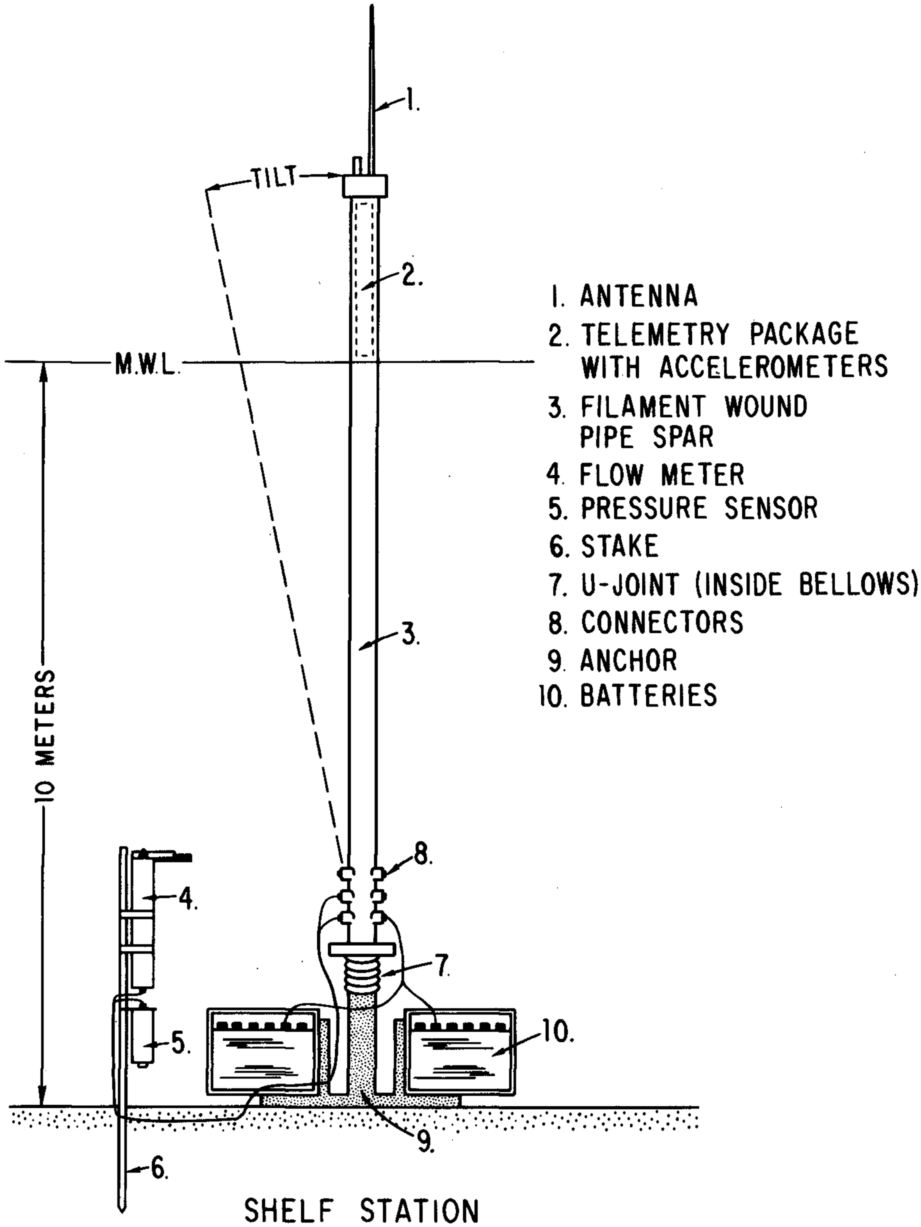

Figure 1. Schematic illustration of the shelf station installation. Tilt angle is measured by accelerometers in top portion of the spar.

To obtain a meaningful resonance curve by sweeping wave frequency, requires that the maximum forcing torque, the restoring moment, the drag coefficient, and the coefficient of inertia remain the same for each driving frequency. These are accomplished by adjusting wave height with frequency to maintain a constant Strouhal number*, and by normalizing the displacements to equivalent maximum acceleration and displaced volume.

Figure 2 gives the resonance curve for angular displacement normalized to the resonant frequency (f_1 = 0.16 Hz) for equivalent maximum acceleration and displaced volume. The curve is of the proper shape and should reflect with some accurancy the resonant frequency of the full size spar. However, the model does not accurately reflect the magnitude of the resonance while constant Strouhal conditions preserve the drag coefficient, the smaller orbital velocities under scaled conditions generate drag torques that are only 2% of what is necessary to compare in scale to those of the full scale spar.

ANALYSIS OF EQUATION OF MOTION

The tilting spar's motion can be described by considering the various forces acting on it. Because the spar is firmly anchored, only forces that produce torques about the universal joints are considered. Four moment producing forces are acting on the spar. A buoyant force acting with a moment arm equal to the distance from the U-joint to the center of buoyancy times the sine of the tilt angle (θ). This moment is represented by the first term on the left hand side of equation (1).

Two forces caused by the waves are represented by the second and third terms of equation (1). The first of these forces is the force that would exist on the water particles within the enclosed volume of the submerged spar in the absence of the spar. This force is distributed along the vertical axis of the spar. The second of the wave generated forces is the virtual mass force, caused by a moving body in an accelerating fluid.

A drag force must also be included which is chosen to be proportional to the square of the relative velocity of the water and the spar. This force is also distributed along the vertical axis of the spar and is represented by the fourth term on the left of equation (1).

These moment producing forces must be balanced by inertial forces which accelerate the spar. The term of the right hand side of equation (1) is the moment of the spar itself.

---

* The Strouhal number is defined as $u_m T/D$ where u_m is the maximum orbital velocity, T is the wave period and D is the spar diameter.

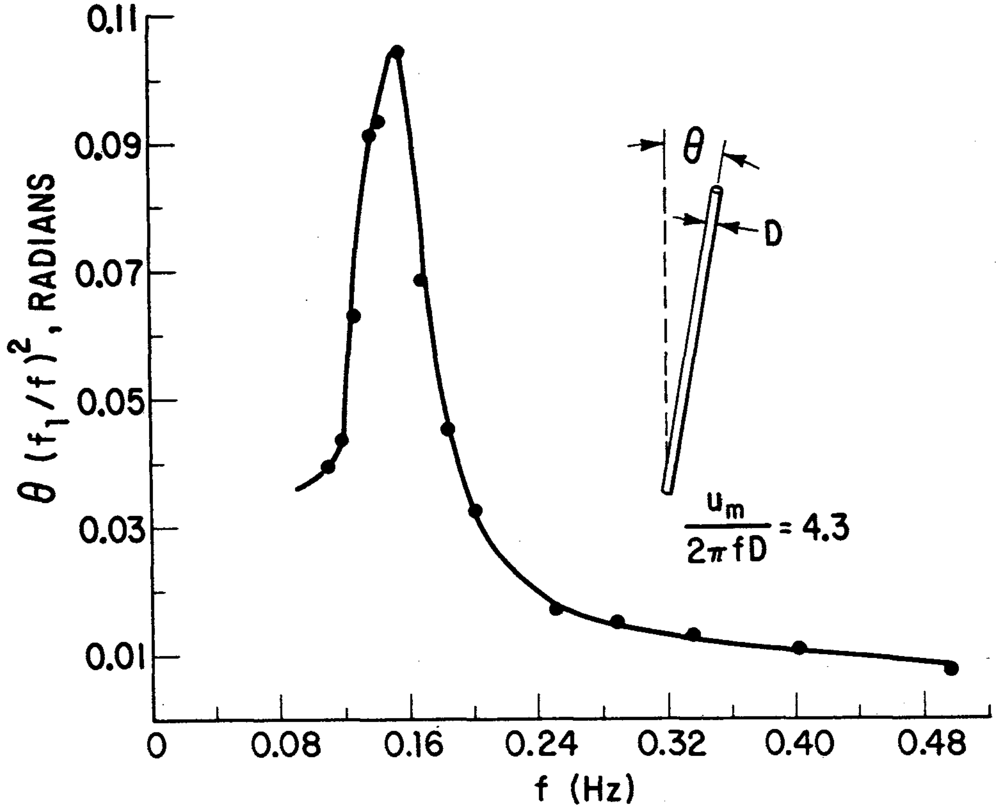

Figure 2. Response curve obtained from 1/7th scale model of spar. Resonance is observed at 0.16 Hz. The magnitude of the resonant peak does not reflect the full scale spar.

$$\sin(\theta) g\, Z_B M_B - \rho a \int_{-h}^{o} \pi r^2 z\, dz - \rho c_a \int_{-h}^{o} (a - \theta z)\, \pi r^2 z\, da$$

$$-1/2\, c_f\, \rho \int_{-h}^{o} |u - \dot{\theta} z|\, (u - \dot{\theta} z)\, 2rz\, dz = -\ddot{\theta}\, I_s \qquad (1)$$

where: θ is the angle of tilt of the spar measured from the vertical, g is the acceleration of gravity, Z_B is the distance from the U-joint to the center of buoyancy, M_B is the net buoyancy, ρ is the density of sea water, u is the horizontal water particle velocity, a is the horizontal water particle acceleration, r is the radius of the spar, z is the distance from the U-joint to any point on the vertical axis, h is the water depth, c_f is the drag coefficient, $\dot{\theta}$ is the angular velocity of the spar, $\ddot{\theta}$ is the angular acceleration of the spar, I_s is the moment of inertia of the spar, and c_m is the virtual mass coefficient.

The equation of motion (1) is a non-linear ordinary differential equation which has been numerically integrated. It was assumed that the spar did not flex and that the velocity profile under the wave was independent of depth (i.e., shallow water wave theory applies). θ was assumed small such that $\sin\theta \approx \theta$. Response of tilt angle versus wave frequency for various maximum orbital velocities were computed. Figure 3 is a plot of these response curves. It is clear from these curves that at high velocities (large waves) resonance is not apparent. At low orbital velocities however, there is a marked resonance occurring at about 0.1 Hz.

MEASUREMENT OF TILT ANGLE

Two accelerometers orthogonally mounted in the top of the spar detect the motion caused by the water movement. For waves with periods ranging from 16 sec to 5 sec, both the acceleration due to gravity and the horizontal motion must be taken into account. Equation (2) describes the acceleration along one axis.

$$a(t) = -g \sin\theta\,(t) + L \frac{d^2\left[\sin\theta\,(t)\right]}{dt^2} \qquad (2)$$

where: a is the measured acceleration, g is the acceleration of gravity, L is the length of the spar, θ is the angle of tilt from the vertical in the x, z plane. $a(t)$ can be expressed as:

$$a(t) = \sum_{n=0}^{k} A_n e^{in\Delta\sigma} \qquad (3)$$

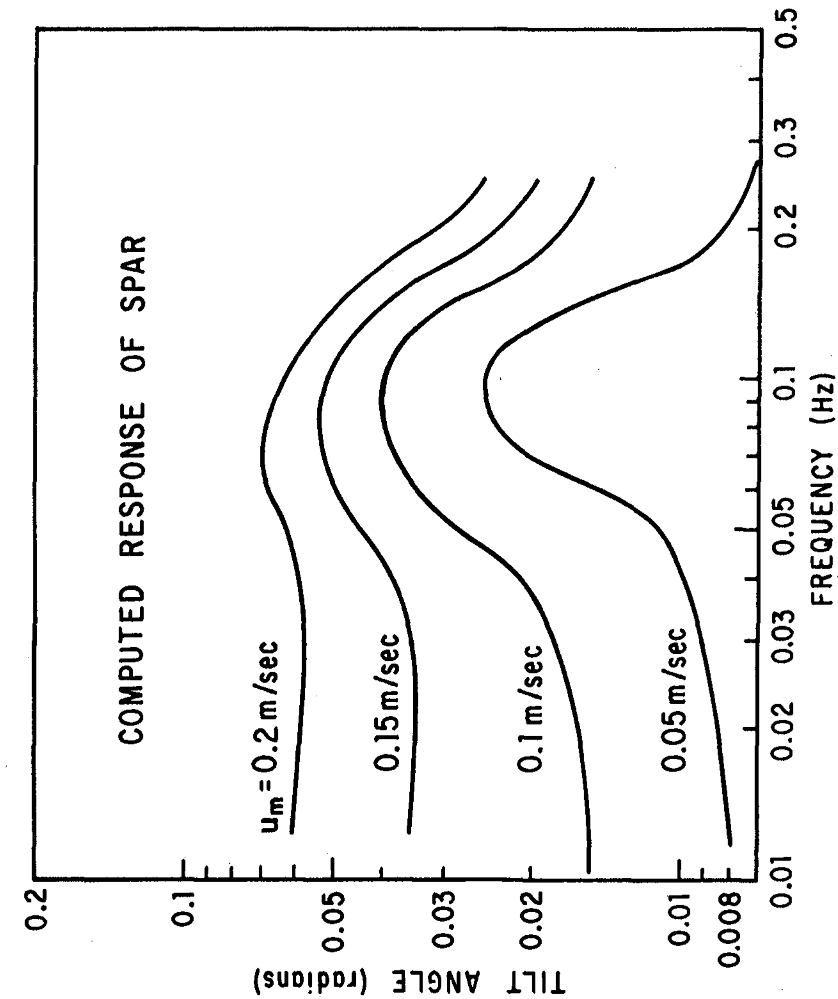

Figure 3. Computed response of the spar for various maximum orbital velocities (U_W). These curves were obtained by integrating equation (1).

where the A_n are the Fourier components, i is $\sqrt{-1}$, k is the number of incremental frequencies, $\Delta\sigma$ is the angular frequency resolution.

Solving equation (2) for each of the coefficients defined in equation (3) gives

$$a(t) = -g \sin\theta_n (t) + L \frac{d^2\left[\sin\theta_n (t)\right]}{dt^2} A_n e^{in\Delta\sigma}$$

let $X_n = \sin\theta_n (t)$

$$\frac{d^2 X_n}{dt^2} - \frac{g}{L} X_n = \frac{A_n}{L} e^{i\Delta\sigma t}$$

The general solution of this differential equation is

$$X_n = B_n e^{i(n\Delta\sigma t + \phi)}$$

where ϕ is an arbitrary phase angle

$$\frac{d^2 X}{dt^2} = -B_n(n\Delta\sigma) e^{i(n\Delta\sigma t + \phi)}$$

substituting for X and $\frac{d^2X}{dt^2}$ gives

$$-B_n(n\Delta\sigma) e^{i(n\Delta\sigma t + \phi)} - \frac{g}{L} B_n e^{i(n\Delta\sigma t + \phi)} = \frac{A_n}{L} e^{in\Delta\sigma t}$$

dividing them by $e^{in\Delta\sigma t}$ and replacing $e^{-i\phi}$ with $(\cos\phi - i \sin\phi)$.

$$-B_n(n\Delta\sigma)^2 - \frac{g}{L} B_n = \frac{A_n}{L} (\cos\phi - i \sin\phi)$$

ϕ can be eliminated by noting $i \sin\phi = 0$; $\phi = 0$. Solving for B_n gives

$$B_n = -\frac{A_n}{g + L(n\Delta\omega)^2}$$

We can now write $\sin\theta_n(t)$ in terms of the Fourier coefficient of $a(t)$:

$$\sin\theta\,(t) = \sum_{n=0}^{k} -\frac{A_n}{g + L(n\Delta\sigma)^2}\, e^{in\Delta\sigma t}$$

With the above procedure the spectra and the time series of the angle of tilt can be obtained from the accelerometer data.

Figure 4 is a plot of the position (in the x-y plane) of the shelf station as a function of time. The predominant motion is on-offshore which is caused by the swell and wind driven wave. However, a longshore motion is also present and has a period on the order of 60 seconds as illustrated in Figure 5.

FIELD MEASUREMENTS

Field data was collected in order to evaluate the computer model outlined above and to determine if the tilt of the spar can be used to determine the direction of wave propagation. The field installation consisted of a line array of four bottom mounted pressure sensors, orthogonally mounted accelerometers in the top of the spar, and a two-component electromagnetic current meter mounted at the base of the station. The axis of the accelerometers were aligned to be 45^{o} with respect to the line array. The current meter was mounted to measure horizontal currents in the on-offshore longshore direction. Data from the sensors was digitized and transmitted to the shore station where it was recorded digitally. A data run consists of 4096 samples from each of the sensors at a rate of 4 samples per second. The site of the installation was off Torrey Pines Beach approximately 3 kilometers north of Scripps Pier in 10 meters of water. These digital data were analyzed using Fast Fourier Transform techniques. Tilt angles were computed as outlines above. Surface wave velocities were computed from the pressure records using linear wave theory. The pressure sensor was located at the base of the spar.

Results from 16 data runs are summarized in Figure 6. Of the four wave periods examined reasonably good agreement was found for wave periods of less than 10 seconds. Poor agreement was found for long period waves. The model predicted tilt angles that are too low by about

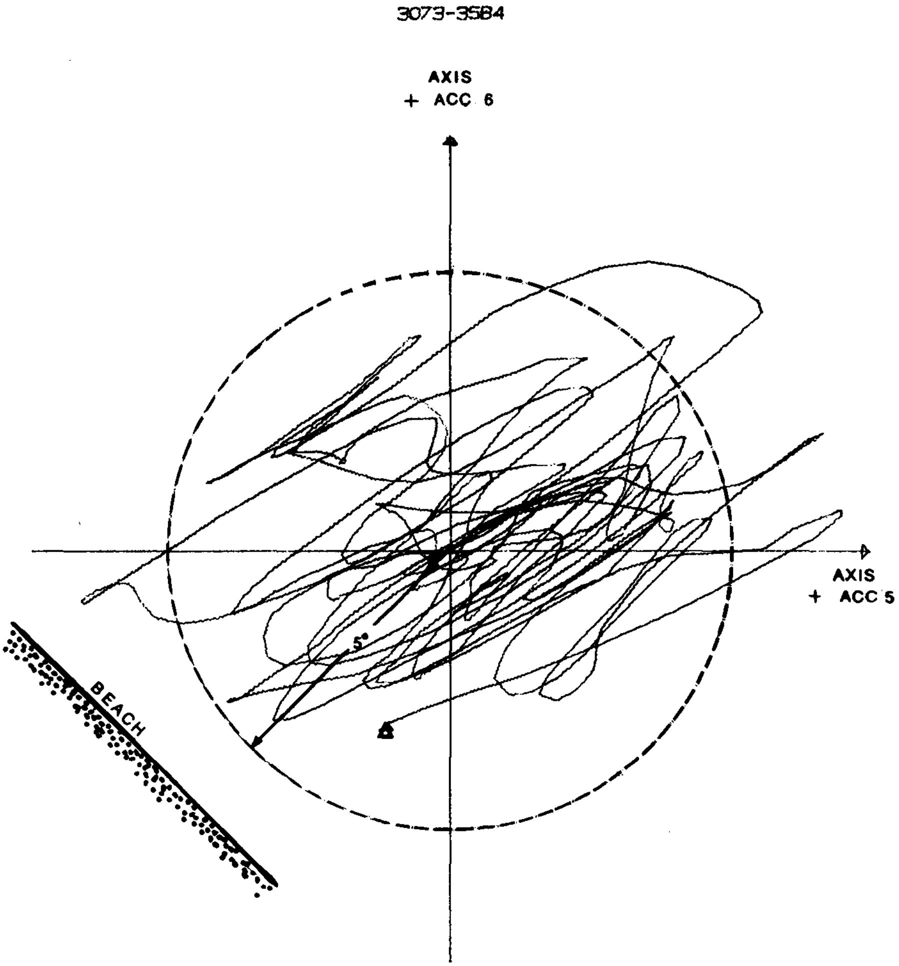

Figure 4. Angle of tilt of the shelf station as derived from the accelerometer data. The predominant on-offshore motion is caused by wind waves and swell. The 5° tilt grid represents a displacement of 0.9 meters from the vertical. Unfiltered loci of motion for 256 seconds of data is represented in this plot. Shelf station was in 10 meters of water on B Range of SIO.

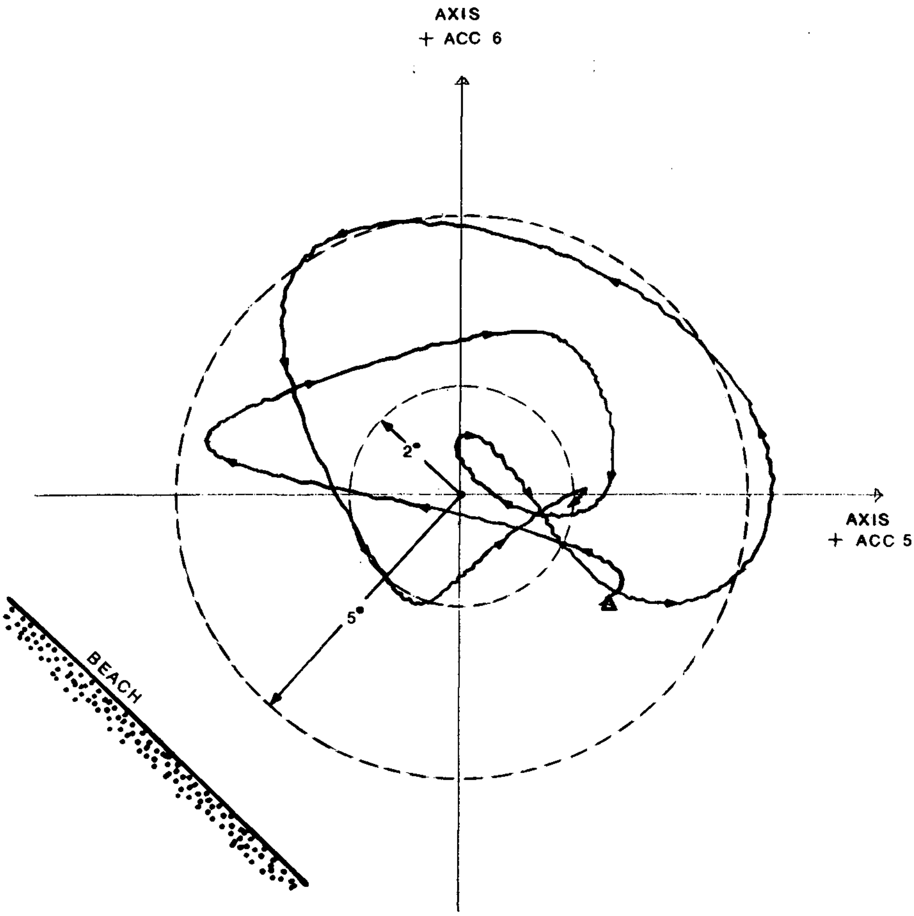

Figure 5. Angle of tilt of the shelf station with the wind waves and swell removed using inverse FFT filter. Only oscillations with periods greater than 40 seconds are shown. This motion is in general agreement with edge wave theory.

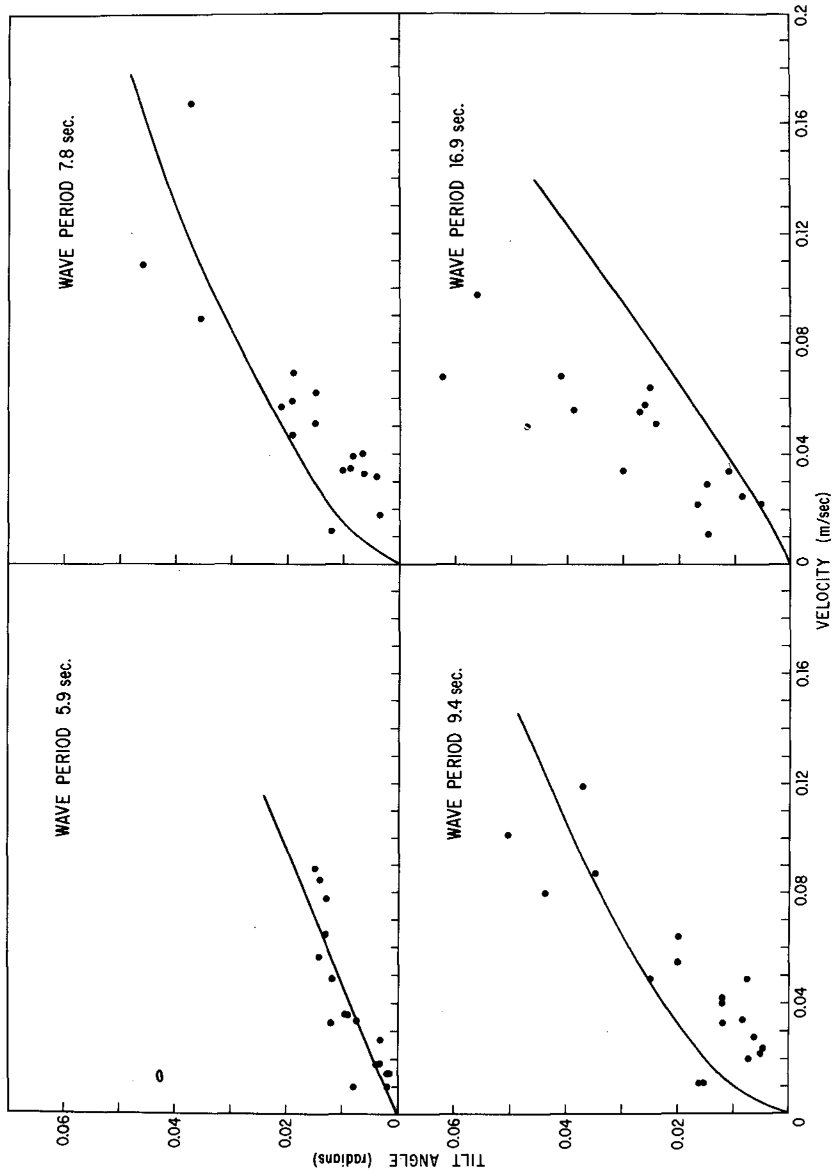

Figure 6. Comparison between predicted tilt angle and measured tilt angle versus velocity for four wave periods. Tilt angle measured using accelerometers. Velocity computed from pressure spectra using linear wave theory.

a factor of two for 17 second waves. The discrepancy is probably caused by the fact that the model treats the drag and inertia coefficients as constants independent of the velocities and wave period. The work of Keulegan and Carpenter (1956) has shown that both the drag coefficient (c_f) and inertia coefficient (c_m) depend on the Strouhal number. At values of the Strouhal number less than 4, the drag coefficient is approximately one and the inertia coefficient approximately two, which are the values used in the computer model. For period parameter values close to 15, c_f increases to approximately two and c_m decreases to less than one

For the long period waves the period parameter does fall into the range where both c_f and c_m can no longer be treated as constants. It would seem therefore, that to predict the current from tilt angle for these long period waves, the computer model must be changed to include variations in these coefficients.

Data from the pressure sensor array was used to determine the direction spectra of the wind waves and swell. The techniques used are described by Pawka (1974). Direction was also obtained using the electromagnetic current meter and a pressure sensor using the techniques developed by Bowden and White (1966). Finally, the direction is estimated using the orthogonal accelerometers.

The analysis techniques for the accelerometer is simply to FFT each accelerometer channel to obtain the spectra values. The estimate of the direction for each frequency band of interest is the vector defined by this orthogonal set of data spectral values.

The comparison of these three methods for obtaining wave direction is contained in Table 1. In general, the three methods agree to within $\pm 5^{\circ}$. When large differences in directional estimates occur it is most likely caused by bimodal direction spectra as indicated by the parameter $P(a_o)$. $P(a_o)$ is a measure of the fit to a unimodal spectra for the array. The smaller $P(a_o)$, the more closely the measure spectral can be represented by a single direction.

RESULTS AND CONCLUSIONS

The main incentive to study the motions of the tilting spar was to ascertain the spectra of the currents driving the system. The analytical expression describing the dynamics of the spar show reasonably good agreement with field measurements for wave periods of less than 10 seconds. It is believed that if the variations in the drag and inertial coefficients are included in the equation, agreement over a wider range of frequency can be obtained.

The generally good agreement obtained between the directional estimates obtained from the spar and the pressure sensor array suggests it can be used in obtaining wave climate. This is based not on the accurancy of the results, but on the reliability of the instrumentation system. In the more than three years the SAS system has been operating,

Table 1. Comparisons of directional information for some November runs. The periods and E_p were obtained from pressure sensor data. Also shown are the angles obtained from current meter data and accelerometer data.

DIRECTION COMPARISONS

RUN	PEAK	PERIOD	$E_p(cm^2)$	ARRAY α_o	ARRAY $P(\alpha_o)$	CURRENT METER α	ACCELER-OMETER α_a
SAS 1-30 Nov 73-01	1	8.8	344	0^o	0.7	2^oS	2^oN
	2	7.4	146	2^oN	5.1	1^oN	3^oN
SAS 1-30 Nov 73-02	1	12.3	118	8^oS	13.0	13^oS	11^oS
	2	7.4	49.8	1^oN	6.8	2^oN	7^oS
SAS 1-04 Nov 73-02	2	14.2	62.3	18^oS	4.3	23^oA	16^oS
	1	6.0	149	1^oS	24.9	11^oS	4^oS
SAS 1-05 Nov 73-02	1	16.8	183	17^oS	3.2	18^oS	15^oS
	2	6.0	156	4^oN	43.1	14^oN	6^oN
SAS 1-08 Nov 73-01	2	14.2	99.2	24^oS	0.6	26^oS	23^oS
	1	9.8	104	2^oN	1.5	4^oS	4^oS
SAS 1-08 Nov 73-03	2	14.2	39.2	25^oS	0.7	27^oS	27^oS
	1	9.8	202	4^oS	15.5	10^oS	9^oS
SAS 1-09 Nov 73-01	1	14.2	85.5	18^oS	2.9	20^oS	21^oS
	2	8.1	60.4	8^oS	53.2	6^oS	9^oS
SAS 1-09 Nov 73-03	2	16.8	42.5	24^oS	0.6	25^oS	21^oS
	1	8.1	60.4	8^oS	53.2	6^oS	9^oS
SAS 1-10 Nov 73-01	2	14.2	67.5	24^oS	0.8	25^oS	16^oS
	1	9.8	284	4^oS	14.0	4^oS	5^oS
SAS 1-10 Nov 73-02	1	10.9	310	8^oS	7.5	16^oS	16^oS
SAS 1-10 Nov 73-04	2	14.2	53.9	24^oS	1.3	27^oS	21^oS
	1	9.8	238	16^oS	18.8	17^oS	15^oS
SAS 1-11 Nov 73-03	2	14.2	26.3	27^oS	0.9	28^oS	21^oS
	1	9.8	370	11^oS	28.2	17^oS	14^oS
SAS 1-11 Nov 73-04	1	8.8	225	26^oS	59.7	17^oS	16^oS
SAS 1-12 Nov 73-01	2	14.2	22.3	25^oS	0.7	28^oS	23^oS
	1	9.8	288	11^oS	32.5	11^oS	10^oS

Definition of Terms:

Peak: In a multi-modal energy spectra the peaks are ordered with respect to their energies.

Period: The modal period for the defined peak of the data of all 4 sensors.

E_p: The energy contained in a spectra peak at 10 m depth, average of the data of all 4 sensors.

α_o: The direction of the best fit to a single wave train for the 4 sensor array measured from the vertical to the array. The fitting technique is based on the minimum value of $P(\alpha_o)$.

α: The angle where the directional spectrum obtained from orbital velocity records reaches a maximum, measure from the normal to the beach, but corrected to the alignment of the array.

α_a: The angle obtained from accelerometer data.

the accelerometer has proven to be the most reliable sensor. The station has proven its integrity by surviving extreme storm conditions. It has proven its ability to remain on station while retaining a size and weight compatible with small boat deployment.

ACKNOWLEDGEMENTS

Development of the SAS system was under sponsorship of the U. S. Department ofCommerce, NOAA, Sea Grant Program. The model study and computer analysis was sponsored by the Office of Naval Research (Geography Programs). Data for the comparison of directional estimates was obtained through a contract with the U. S. Army Corps of Engineers, Coastal Engineers Research Center.

The authors wish to thank the students and staff of the Shore Processes Study Group, Scripps Institution of Oceanography for their help and support of this study. We are especially indebted to Mr. Scott Jenkins for performing the model study.

REFERENCES

Bowden, K. F. and R. A. White, 1966, "Measurement of the orbital velocities of sea waves and their use in determining the directional spectrum", Geophysical Jour. Roy. Astronomical Soc., vol 12, p. 33-54.

Keulegan, G. H. and L. H. Carpenter, 1956, "Forces on cylinders and plates in an oscillating fluid", National Bureau of Standards, Report 4821, 31 pp., 28 figs.

Lowe, R. L., D. L. Inman and B. M. Brush, 1973, "Simultaneous data system for instrumenting the shelf", 13th International Conf. Coastal Eng., Amer. Soc. Civil Eng., p. 95-112.

Pawka, S. S., 1974, "Study of wave climate in nearshore waters", Proc. in the International Symposium on Ocean Wave Management and Eng., vol 1, p. 745-760.